CLIMATE MODEL TESTING WITH GPS RADIO OCCULTATION DATA

Director's Research and Development Fund (DRDF)
Final Report

JPL Task #1322

Chi O. Ao (PI), Tracking Systems and Applications Section (335)
James G. Anderson (Co-PI), Harvard School of Engineering
and Applied Science, Harvard University
Stephen S. Leroy, Harvard School of Engineering and Applied Science,
Harvard University

A. OBJECTIVES

GPS radio occultation (RO) measurements have been known to possess characteristics that make them particularly suitable for climate benchmarking [1]. In this study, we explored the application of GPS RO data in climate model testing. In order to facilitate comparisons with climate models, a Bayesian method was first applied to interpolate the quasi-randomly distributed RO measurements onto regular latitude–longitude grids. The 8-year continuous time series of RO measurements from the CHAllenging Minisatellite Payload (CHAMP) and Constellation Observing System for Meteorology, Ionospheric, and Climate (COSMIC) satellite missions were calculated and compared with the European Centre for Medium-range Weather Forecast (ECMWF) reanalysis and the climate models from the Fourth Scientific Assessment of the Intergovernmental Panel for Climate Change (IPCC AR4).

B. APPROACH AND RESULTS

1. Data Description

To obtain over 8 years of continuous RO measurements, we used data from both the CHAMP (April 2001–August 2008) and COSMIC (also known as FORMOSAT-3, June 2006–present) missions. The CHAMP mission yielded approximately 150 profiles per day over the globe, with local time sampling that repeats approximately every 4 months. With six satellites capable of performing both rising and setting occultations, COSMIC data provided an order-of-magnitude improvement in throughput as well as excellent diurnal cycle sampling. The period of overlap between the CHAMP and COSMIC data allowed us to assess sampling error from the more limited coverage of the CHAMP data.

The CHAMP and COSMIC data were retrieved at JPL [2]. Each occultation yields a vertical profile of refractivity with high vertical resolution (approximately 200 m up to the lower stratosphere). The refractivity can be expressed as a function of temperature, pressure, and water vapor. By neglecting water vapor, the temperature and pressure can be obtained directly from the hydrostatic equation. The temperature and pressure thus derived are referred to

as the "dry" temperature (Tdry) and "dry" pressure (Pdry). They differ from the physical temperature and pressure only when water vapor is abundant (below about 8 km altitude in the tropics).

2. Data Gridding with Bayesian Interpolation Method

To perform climate averaging with the GPS RO data and to compare with climate models, it is convenient to first interpolate the quasi-randomly distributed measurements onto a regular latitude–longitude grid. In this study, the gridding was carried out within the framework of Bayesian interpolation [3]. The Bayesian interpolation method uses a set of basis functions to fit irregularly sampled data with unknown noise characteristics and represents a generalized least χ^2 method. What makes this approach Bayesian is its use of a regularizing function that is weighted optimally against data misfit to resolve structures in the data without overfitting. For interpolation on a sphere, we used spherical harmonic functions as the basis functions. The regularizer functions were chosen to be simple power laws that assigned larger penalties to spherical harmonics with larger degrees and non-zonal orders ($m \neq 0$) [3].

Figure 1 illustrates an example of the Bayesian interpolation of GPS RO data. In this example, the temperature data at 10 km height level from January 1–4, 2007, were fitted with spherical harmonic functions up to degree 8. Having obtained the fitting coefficients, the temperature at any latitude and longitude can be easily and quickly computed. Here, the interpolated temperature was calculated on a 10 deg × 10 deg latitude–longitude grid. Figure 1a shows the interpolated COSMIC temperatures in contour, while Figure 1b shows the estimated error from the Bayesian interpolation that characterizes the global misfit. The actual locations of the measurements are shown in dots. Note that the estimated error is larger in the tropics due to the smaller number of measurements present in the tropics. However, regional variability is not accounted for in this formulation, so the error tends to be overestimated in the tropics where the synoptic variability is lower. Figure 2 shows the zonal averages from COSMIC and CHAMP for the same period. The zonal averages can be easily calculated by summing over the spherical harmonic functions with zero order. It can be seen that due to the tenfold increase in the COSMIC measurements, the estimated interpolation error is smaller by a factor of about 3.

To calculate monthly averages, we first divided the data into bins of ~3 days each. We note that bins with too few days would have an insufficient number of measurements that caused overfitting, while bins with too many days would have increased natural variability that caused underfitting. This suggests that there should exist an optimal bin size for a given sampling density. In practice, however, we found that the results were not very sensitive to the choice of the bin size. We applied the Bayesian interpolation for each of the 3-day bins and interpolated the measurements to a gridded dataset. The gridded data from each of the bins within a month were then averaged at each grid point to obtain a monthly average. To better quantify the sampling error, we performed sampling analysis using the ECMWF gridded data. The ECMWF data were first subsampled at the GPS RO times and locations. The subsampled data were then interpolated and compared against the derived monthly average obtained with the full ECMWF data. For COSMIC sampling density, the global temperature RMS difference was found to be on the order of 0.3 K.

3. Time Series Analysis and Comparison with Climate Models

The time series of the Pdry from GPS RO was analyzed and compared with climate models. The change in the log(Pdry) is directly related to the change in geopotential height [1]. As such, it represents the layer-averaged temperature below a particular altitude. Figure 3 shows the monthly zonally averaged Pdry at 10 km altitude for 50 N and 50 S latitudes. The dry pressure exhibits clear annual cycles that correspond to the warming and cooling of the troposphere. Figure 3 also shows the monthly Pdry anomalies with the annual cycles removed. During the period when data from both CHAMP and COSMIC were available, the results agreed well with each other, despite the fact that COSMIC had about 10 times more profiles. This suggests that CHAMP provided adequate sampling for studying monthly zonal means. For comparison, corresponding results from ERA-interim are also shown in Figure 3. The agreement between GPS RO and ERA-interim is quite good.

We performed linear regression analysis on the log(Pdry) anomalies in the period of 2001–2009 (CHAMP from 2001–2006 and COSMIC from 2007–2009). Figure 4 shows the linear trends obtained from GPS RO data for 50 N and 50 S at 10 km height level and how these trends compare with ERA-interim and an ensemble of IPCC AR4 climate models with SRES A1B greenhouse gas forcing scenario. These results show that (1) there are broad agreements between GPS RO, ERA-interim, and most of the models, and (2) the trends obtained this period are not statistically significant.

Figure 5 shows the global annual average of log(Pdry) from 2002–2009 at 20 km height level. The approximate pressure scale height of 5000 m has been multiplied to convert log(Pdry) to layer thickness (cf. Eq. 6 of [1]). In addition to simple global averaging, we have also computed an "optimized" average using the optimal fingerprinting technique ([1] and references therein), where the climate models had been used to infer the natural variability. In this case, there appears to be very little difference between the simple and optimized averages. To relate the changes in the troposphere thickness with surface temperature, we included the Hadley Center/University of East Anglia Climate Research Unit (HadCRUT3) [4] temperature data record from 2000–2009 in Figure 5. These results showed an interesting divergence between the troposphere thickness and surface temperature in the last few years. Further analysis on the GPS RO interpolation and sampling errors should be carried out in the future to assess the statistical significance of such differences.

C. SIGNIFICANCE OF RESULTS

This study demonstrated the potential values of GPS RO in climate model testing. We developed and implemented an approach to grid the GPS RO retrieved profiles to facilitate comparisons with models. The tools and analyses developed in this study will be useful not only in climate model testing but also in delineating the sampling accuracy and characteristics of GPS RO missions that are currently in planning, such as CLARREO and other National Research Council Decadal Survey missions, where NASA/JPL is expected to be actively involved.

D. FINANCIAL STATUS

The total funding for this task was $120,000, of which $101,074 has been expended.

E. ACKNOWLEDGEMENTS

We wish to thank Martin Lo and Taktin Oey for their contributions to the Bayesian interpolation work at JPL.

F. PUBLICATIONS

None

G. REFERENCES

[1] S. S. Leroy, J. G. Anderson, and J. A. Dykema, "Testing Climate Models Using GPS Radio Occultation: A Sensitivity Analysis," *J. Geophys. Res*. **111**, (2006): D17105. doi:10.1029/2005JD006145

[2] G. A. Hajj, E. R. Kursinski, L. J. Romans, W. I. Bertiger, and S. S. Leroy, "A Technical Description of Atmospheric Sounding by GPS Occultation," *J. Atmos. Solar-Terr. Physics* **64** (2000): pp. 451–469.

[3] S. S. Leroy, "Measurement of Geopotential Heights by GPS Radio Occultation," *J. Geophys. Res*. **102** (1997): pp. 6971–6986.

[4] P. Brohan, J. J. Kennedy, I. Harris, S. F. B. Tett, and P. D. Jones, "Uncertainty Estimates in Regional and Global Observed Temperature Changes: A New Dataset from 1850," *J. Geophys. Res.* **111** (2006): p. D12106. doi:10.1029/2005JD006548

H. FIGURES

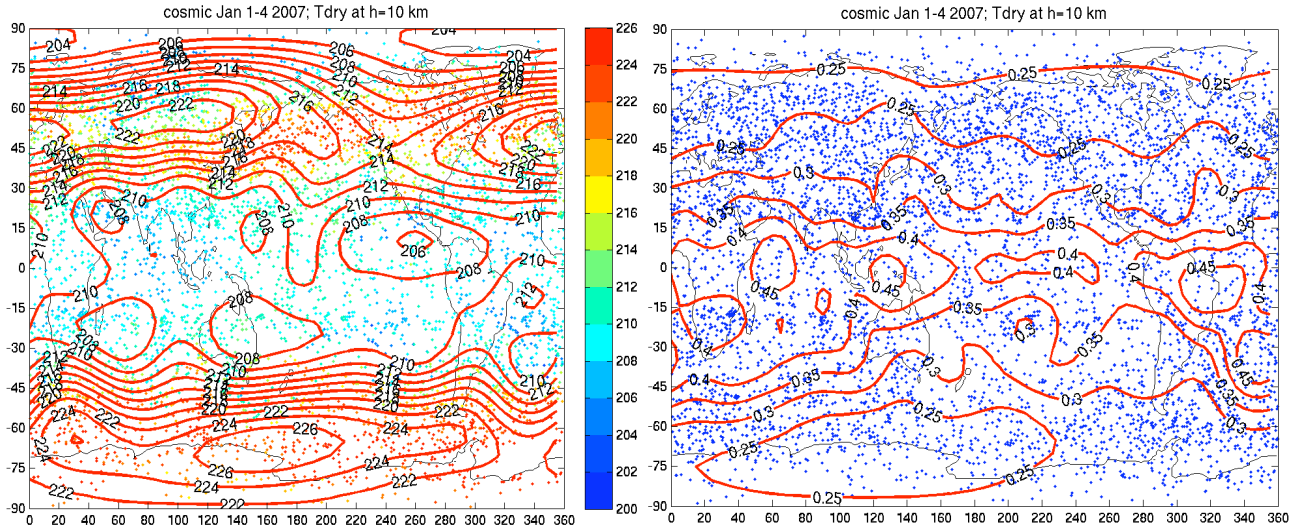

(a) Interpolated temperature [K] **(b) Estimated interpolation error [K]**

Figure 1. Bayesian interpolation of COSMIC temperature data at 10 km from January 1–4, 2007. (a) Contours from the interpolated temperature. The dots refer to the individual occultation locations and temperature values with color scales shown on the right. (b) Estimated interpolation error. The dots refer to the individual occultation locations.

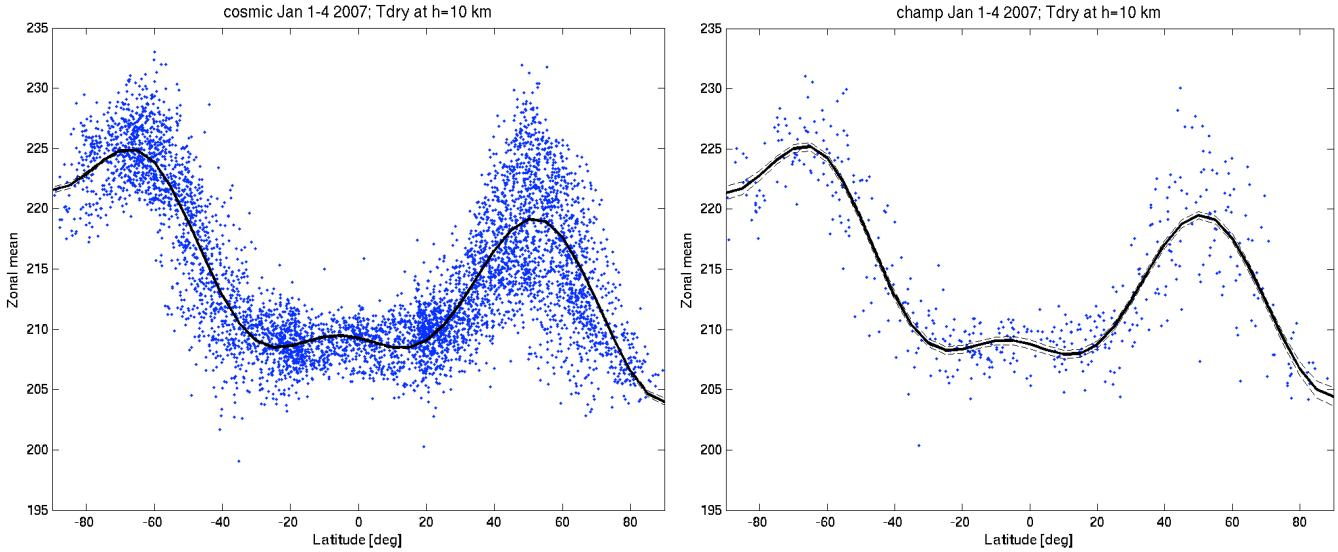

(a) Zonal mean from COSMIC [K] **(b) Zonal mean from CHAMP [K]**

Figure 2. Zonal averages of GPS RO temperature from (a) CHAMP and (b) COSMIC at 10 km from January 1–4, 2007. Solid lines represent the interpolated temperatures and dashed lines represent the estimated interpolation errors. Dots show the actual occultation data.

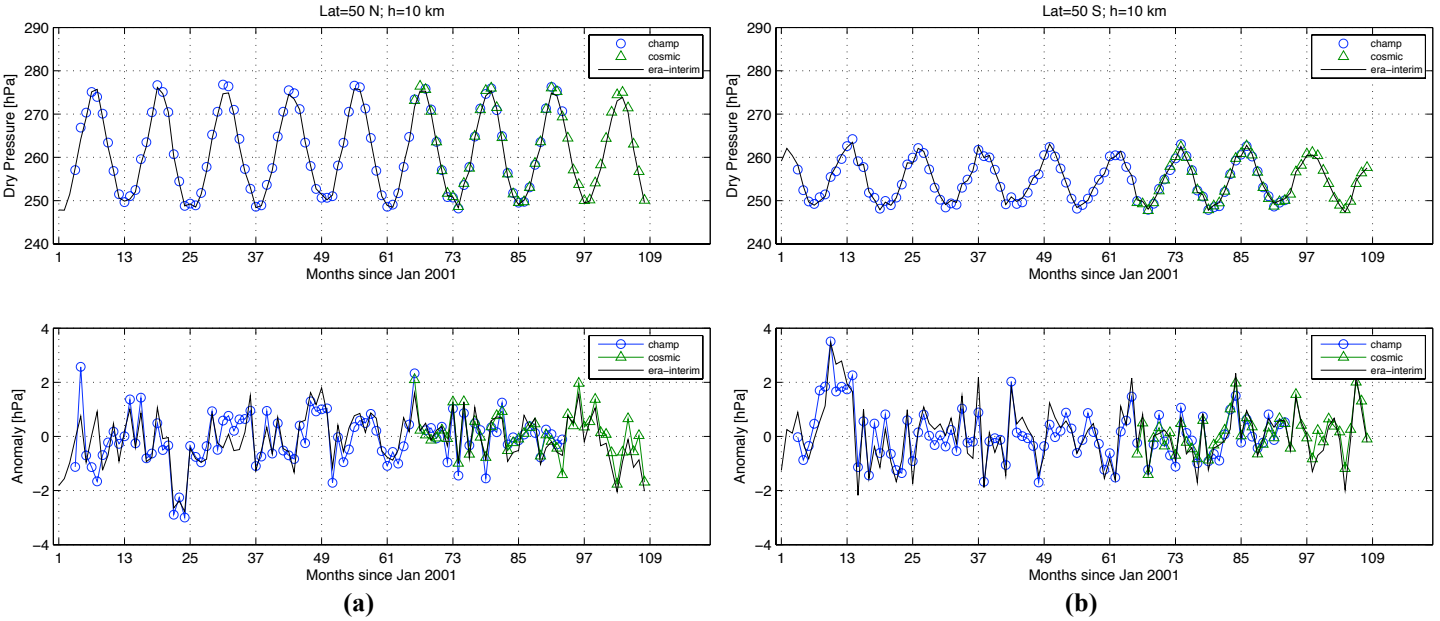

Figure 3. Time series of monthly zonal means of the dry pressure at 10 km obtained from CHAMP (April 2001-August 2008 with July 2007 missing) and COSMIC (June 2006–Dec. 2009) at (a) 50 N latitude and (b) 50 S latitude. For comparison, the corresponding results from ERA-interim are shown. Lower panels show the monthly dry pressure anomalies obtained by removing the annual cycles.

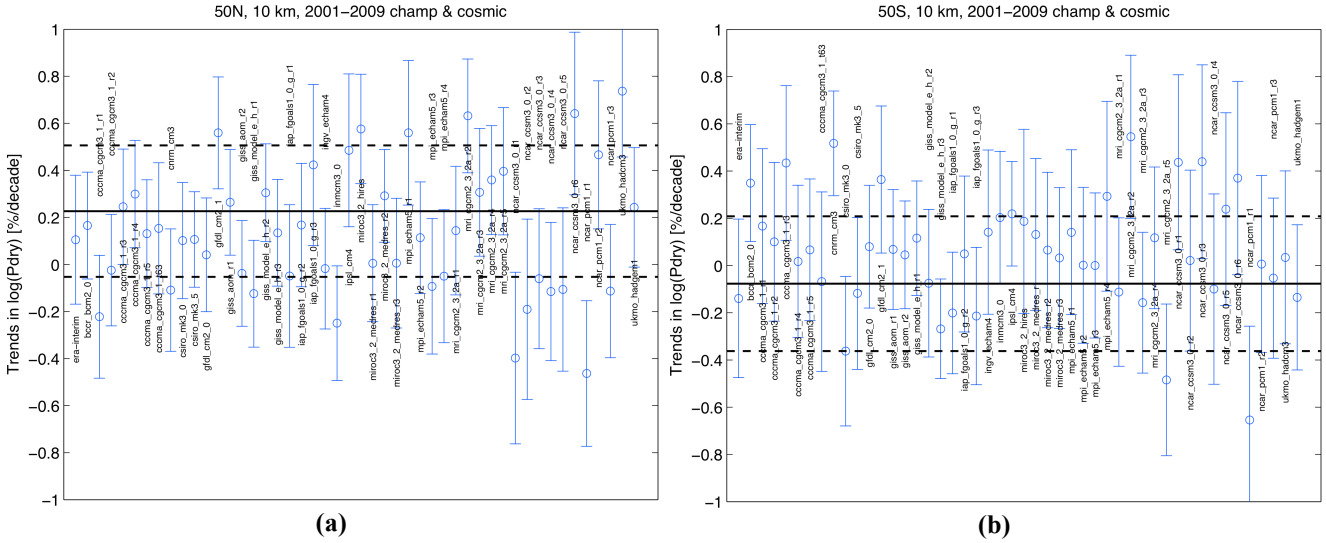

Figure 4. Linear trends in log(Pdry) at 10 km height over 2001–2009 from GPS RO data compared with ERA-interim and IPCC AR4 climate models. (a) 50N; (b) 50 S. Solid black lines denote the trends, while the dashed lines denote the 95% confidence intervals. The corresponding ERA-interim and IPCC model results are shown as circles with error bars denoting the 95% confidence intervals.

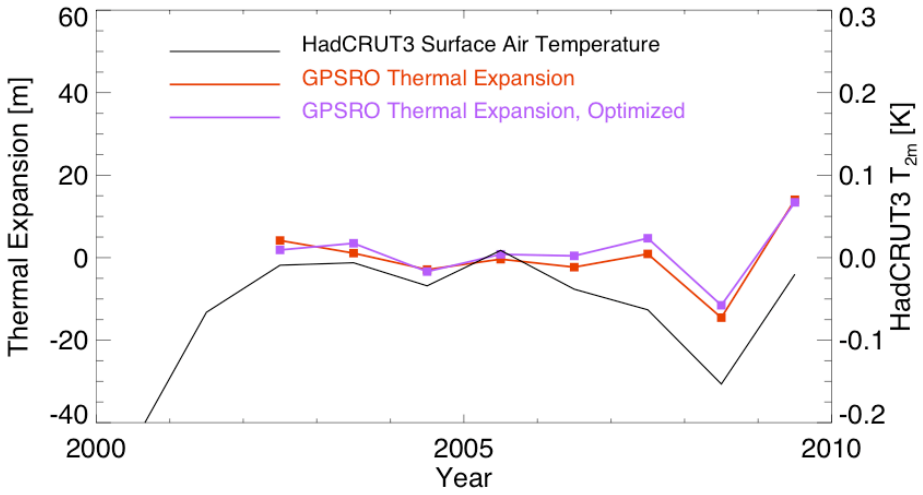

Figure 5. Troposphere thermal expansion inferred from GPS RO log(Pdry) data compared with surface temperature data from HadCRUT3.